

Showcasing research from the groups of Professor Karl S. Ryder, Professor A. Robert Hillman and Professor Andrew P. Abbott at the Materials Centre in the School of Chemistry, University of Leicester, Leicester, United Kingdom.

Amidine-based ionic liquid analogues with  $\text{AlCl}_3$ : a credible new electrolyte for rechargeable Al batteries

The electrochemical performance of amidine-based ionic liquid analogues has been examined for aluminium battery applications. These electrolytes can compete with current state-of-the-art chloroaluminate ionic liquids at a significantly lower economic cost of the starting materials.

As featured in:



See Anthony J. Lucio *et al.*,  
*Chem. Commun.*, 2021, **57**, 9834.



Cite this: *Chem. Commun.*, 2021, 57, 9834

Received 21st May 2021,  
Accepted 18th August 2021

DOI: 10.1039/d1cc02680a

rsc.li/chemcomm

## Amidine-based ionic liquid analogues with $\text{AlCl}_3$ : a credible new electrolyte for rechargeable Al batteries†

Anthony J. Lucio,<sup>a</sup> Igor Efimov,<sup>a</sup> Oleg N. Efimov,<sup>b</sup> Christopher J. Zaleski,<sup>c</sup> Stephen Viles,<sup>a</sup> Beata B. Ignatiuk,<sup>a</sup> Andrew P. Abbott,<sup>a</sup> A. Robert Hillman<sup>a</sup> and Karl S. Ryder<sup>a</sup>

**Here we demonstrate the generation of novel ionic liquid analogue (ILA) electrolytes for aluminium (Al) electrodeposition that are based on salts of amidine Lewis bases. The electrolytes exhibit reversible voltammetric plating/stripping of Al, good ionic conductivities ( $10\text{--}14\text{ mS cm}^{-1}$ ), and relatively low viscosities ( $50\text{--}80\text{ cP}$ ). The rheological properties are an improvement on analogous amide-based ILAs and make these liquids credible alternatives to ILAs based on urea or acetamide, or conventional chloroaluminate ionic liquids (IL) for Al battery applications.**

The focus of this communication is on the exploration of new and novel electrolytes based on the  $\text{HCl}$  salts of a range of amidine species. Amidines are a class of organic species related to amides, where the O atom has been replaced with an  $\text{sp}^2$  N atom. Recent studies have demonstrated that in the case of amide-based ILAs (e.g. those based on acetamide or urea), the interaction between the  $\text{AlCl}_3$  Lewis acid and the amide base likely occurs through an Al–O bond,<sup>1,2</sup> consistent with the fact that  $\text{AlCl}_3$  is highly oxophilic. However, O-based ligands to Al are strongly bound, resulting in slow exchange kinetics that limit the electrochemical reduction and deposition of Al metal. While this is not a kinetic study, our strategy here has been to replace the O atom of the amides with an N atom giving a structurally similar environment where only N-coordination is possible. In addition, unlike amides, amidines can be easily protonated facilitating the delocalisation of electron density across the N-centres. In the case of the guanidinium cation, the

three N-centres become equivalent by virtue of their resonance forms (ESI† 2, Fig. S1). These cationic amidinium species are consequentially softer Lewis bases than the analogous amides and therefore, we propose, ligands that are more facile. Additionally, they contribute to the conductivity of the liquids through their positive charge. Specifically, this is the first report to our knowledge of ILAs made from Lewis basic salts of guanidinium chloride (Guan-Cl), acetamidinium chloride (Acet-Cl) and formamidinium chloride (Form-Cl). For comparative purposes, we have included data for the IL, 1-butyl-1-methylpyrrolidinium chloride (BMP-Cl).

The rapidly increasing demand for rechargeable battery systems in order to power stationary energy storage, mobile electronics and electric vehicles has generated acute technical and social challenges. Significant research and development has been reported on lithium-, sodium-, and magnesium-based battery technologies, with lithium-ion batteries (LIB) dominating the market share. Although LIBs are widely used in everyday technology they possess drawbacks that need to be addressed e.g. diminishing supply of source materials, difficulty in recycling used battery systems,<sup>3</sup> and safety concerns (i.e. thermal runaway and leakage of hazardous components).<sup>4</sup> As a result, there are major efforts to develop battery systems to compete with and replace current technology. Even if new battery chemistries cannot match LIB performance metrics, the possibility of cheaper, safer and more environmentally friendly options motivate research in this field.

A very encouraging option are Al-based batteries.<sup>5</sup> Al is inexpensive, highly abundant, and possesses an energy density close to Li.<sup>6</sup> Like Li, however, Al systems require non-aqueous chemistries, as the reduction potential of Al is more negative than that for hydrogen evolution in aqueous-based electrolytes. The development of non-aqueous electrolytes for Al battery systems has subsequently received significant attention, although much of this has only occurred relatively recently.

The electrolyte component of a battery is fundamental to its performance, and developing electrolytes with low viscosity,

<sup>a</sup> Materials Centre, School of Chemistry, University of Leicester, Leicester LE1 7RH, UK. E-mail: a.j.l71@le.ac.uk

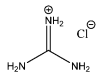
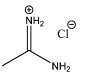
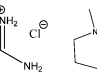
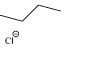
<sup>b</sup> Russian Acad. Sci., Inst. Prob. Chem. Phys., 1 Acad. Semenov Ave, Chernogolovka 142432, Moscow Region, Russia

<sup>c</sup> Wolfson School of Mechanical Electrical & Manufacturing Engineering, Loughborough University, Loughborough LE11 3TU, UK

† Electronic supplementary information (ESI) available: Experimental section (ESI 1), resonance forms of guanidinium cation (ESI 2), <sup>27</sup>Al NMR spectra (ESI 3), CV cycles (ESI 4), *i*-*E* curve fitting (ESI 5), Arrhenius Plots (ESI 6), charge-discharge curves (ESI 7), and SI references (ESI 8). See DOI: 10.1039/d1cc02680a



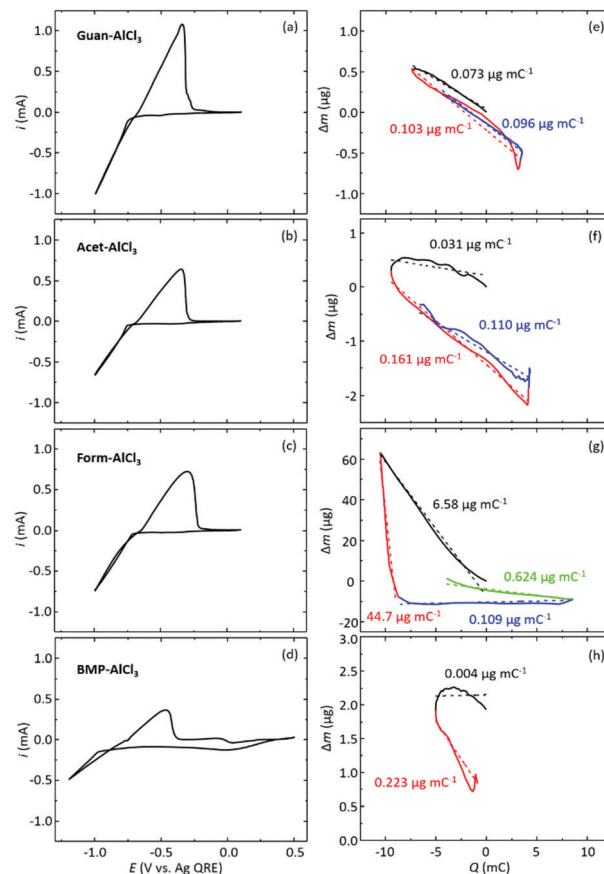
**Table 1** Chemical structure of the Lewis base, electrolyte acronym, electrolyte molar composition, and [Al]

Lewis base chemical structure				
Acronym	Guan-AlCl <sub>3</sub>	Acet-AlCl <sub>3</sub>	Form-AlCl <sub>3</sub>	BMP-AlCl <sub>3</sub>
Mole Ratio AlCl <sub>3</sub> :base	2.5 : 1	1.5 : 1	1.5 : 1	1.5 : 1
[Al] / mol dm <sup>-3</sup>	7.7	6.7	7.1	5.2

high ionic conductivity, a large polarisable potential window and good thermal stability are all important characteristics. To date, chloroaluminate electrolytes from imidazolium<sup>7–9</sup> and pyrrolidinium-based<sup>10–12</sup> salts have been studied but they are often costly. ILAs also known as deep eutectic solvents (DES), which are formed by mixing a Lewis acid (*e.g.* AlCl<sub>3</sub>) and a Lewis base (*e.g.* urea) at a desired mole ratio, have been recently explored as they are inexpensive, very easy to synthesize and can be made from abundant often non-toxic materials. In a manner similar to ILs, the Lewis base can be selected to generate a range of different ILAs with AlCl<sub>3</sub>, thus facilitating control of the physiochemical properties of the electrolyte. At present urea<sup>13–16</sup> and acetamide<sup>17–22</sup> (and their derivatives) have been explored, however, there is still significant room for improvement with electrolyte development.

The chemical structures of the different amidine salts studied here (Guan-Cl, Acet-Cl, Form-Cl, and BMP-Cl) are shown in Table 1 along with the stoichiometric ratios and molar concentrations of Al in each liquid. The structures represent a sequential substitution of the parent amidine cation, R-(C=NH<sub>2</sub><sup>+</sup>)-NH<sub>2</sub> where R = NH<sub>2</sub>, CH<sub>3</sub> and H. The variants where R' = CH<sub>3</sub> and NH<sub>2</sub> in R'-(C=O)-NH<sub>2</sub> are acetamide and urea, respectively. The liquid formulations shown were all stable at room temperature (291 K); of particular note is the high concentration of Al achieved with Guan-AlCl<sub>3</sub> that is facilitated by the presence of three N-based coordination sites.<sup>27</sup> Al NMR spectra of these electrolytes indicate that a mixture of anionic and cationic Al species are present (ESI† 3, Fig. S2). Whilst we were able to make liquid formulations of the Acet-AlCl<sub>3</sub> and Form-AlCl<sub>3</sub> based liquids with higher AlCl<sub>3</sub> content (*e.g.* at a mole ratio of 2:1), some of these formed glassy solids on cooling under ambient conditions.

The cyclic voltammograms (CV) of the different electrolytes were recorded at 18 ± 1 °C with the Pt coated face of a 10 MHz AT-cut quartz crystal, Fig. 1(a–d). In all cases, these show cathodic current associated with Al<sup>3+</sup> reduction, an anodic peak corresponding to the dissolution of Al metal, evidence of a nucleation loop, and are commensurate with the chemically reversible plating and stripping of Al. The CVs show the second cycle and we find little difference in the voltammograms of successive CV cycles (ESI† 4, Fig. S3). The *i*(*E*) traces also show striking linearity in the region of cathodic current and in the first part of the anodic stripping peak. This characteristic

**Fig. 1** CVs (2<sup>nd</sup> cycle) for (a) Guan-AlCl<sub>3</sub>, (b) Acet-AlCl<sub>3</sub>, (c) Form-AlCl<sub>3</sub>, and (d) BMP-AlCl<sub>3</sub> liquids (electrode area = 0.21 cm<sup>2</sup>, scan rate = 20 mV s<sup>-1</sup>, *T* = 18 ± 1 °C). EQCM plots are shown in (e–h).

response in the stripping peak has also been seen for pyrrolidinium<sup>11,23</sup> and urea-based<sup>22</sup> electrolytes. In addition, no cathodic reduction peak is observed for these CVs in the potential region shown. Taken together, these observations indicate that the reduction of Al<sup>3+</sup> (and subsequent deposition of Al metal), is not mass-transport limited in any of these liquids. Numerical integration of the cathodic (*Q*<sub>red</sub>) and anodic stripping (*Q*<sub>ox</sub>) portions of the voltammograms (Fig. 1) shows that for the amidine liquids, the processes are equivalent with a ratio, *Q*<sub>red</sub>/*Q*<sub>ox</sub>, of unity. The corresponding value for the BMP-AlCl<sub>3</sub> liquid is lower, at 0.89.

For the three amidine liquids, the onset potential for Al<sup>3+</sup> reduction is close to −0.75 V, whereas that for BMP-AlCl<sub>3</sub> is closer to −1.0 V, hence the modified potential range examined. Correspondingly, the anodic peaks for the amidine liquids are both sharper in appearance and larger in magnitude than that of the BMP-AlCl<sub>3</sub> liquid. These observations are in part related to the relative concentrations of Al<sup>3+</sup> in the liquids (Table 1) and in part due to the differences in rheological properties (discussed below) of the liquids. However, we can conclude from these data that under equivalent conditions of time (potential scan rate) and temperature, all of the amidine liquids perform better than the BMP-AlCl<sub>3</sub> system where Guan-AlCl<sub>3</sub> exhibits the largest anodic and cathodic responses.





The plating and stripping of Al species on the Pt electrode can also be visualised from electrochemical quartz crystal microbalance (EQCM) curves. The EQCM data, plotted as the relative change in mass ( $\Delta m$ ) as a function of charge ( $Q$ ), are presented in Fig. 1(e–h). For a faradaic process we would expect these plots to be linear, with a theoretical slope,  $\Delta m/Q$ , defined by the Sauerbrey equation to be  $0.093 \mu\text{g mC}^{-1}$ . Here, a range of deviations from linear behaviour (not predictable on the basis of  $i(E)$  responses) are observed. Average  $\Delta m/Q$  ratios for selected charge ranges within the full voltammetric cycle are indicated by annotated values colour coded to corresponding data ranges in Fig. 1(e–h). The Guan- $\text{AlCl}_3$  electrolyte (Fig. 1e) most closely follows the faradaic response with  $\Delta m(Q)$  traces having values close to the theoretical slope;  $0.073 \mu\text{g mC}^{-1}$  and  $0.096 \mu\text{g mC}^{-1}$  (plating), and  $0.103 \mu\text{g mC}^{-1}$  (stripping). Similarly, Acet- $\text{AlCl}_3$  (Fig. 1f) shows  $0.031 \mu\text{g mC}^{-1}$  and  $0.110 \mu\text{g mC}^{-1}$  (plating), and  $0.161 \mu\text{g mC}^{-1}$  (stripping). Small, negative deviations from the theoretical slope usually indicate that less mass is deposited on the electrode crystal than is expected. Based on charge this can be due to minor side-reactions or impurities, but as with any surface-sensitive measurement, one cannot exclude them without further quantitative study. However, the larger deviations and non-linear responses for Acet- $\text{AlCl}_3$  ( $0.031 \mu\text{g mC}^{-1}$ ), Form- $\text{AlCl}_3$  (Fig. 1g), and BMP- $\text{AlCl}_3$  (Fig. 1h) liquids suggest non-gravimetric, local rheological changes occurring at the electrode/electrolyte interface commensurate with changes in Al ion concentration during the redox cycle. In the case of the Form- $\text{AlCl}_3$  liquid (Fig. 1g) the apparent mass changes throughout the electrochemical plating/stripping process are very large, and indicates that a phase transformation (*e.g.* electrolyte gelification) may be occurring locally within the diffusion layer during the electrodeposition process at negative potentials.

The deviation of the Form- $\text{AlCl}_3$  data can also be observed in the acoustic loss data gathered from EQCM. The real component of the acoustic impedance (loss) response, which is related to the resistance,  $R_q$ , can be estimated from the width of the resonance frequency peak at half height,  $W$ , using eqn (1):

$$R_q = 2\pi L W \quad (1)$$

where  $L$  is the inductance (units of Henry, H).<sup>24,25</sup> Water has a known viscosity and acoustic loss that can be used as a calibration reference, and for a 10 MHz quartz crystal resonator and  $R_q = 220 \Omega$  we find  $L = 0.008 \text{ H}$ . This  $L$  value was used to estimate the ILA electrolyte  $R_q$  values. The acoustic losses ( $R_q$ ) measured as a function of potential during the EQCM measurements are shown in Fig. 2 for the different electrolytes. Acet- $\text{AlCl}_3$  (pink short-dotted trace), BMP- $\text{AlCl}_3$  (blue dash-dotted trace), and Guan- $\text{AlCl}_3$  (red dashed trace) show a constant resistance (on this scale) around  $2 \text{ k}\Omega$  throughout the entire potential sweep negative and positive. On the other hand, Form- $\text{AlCl}_3$  (black solid trace) shows a more than double increase in resistance within the potential region (*i.e.*  $-0.5 \text{ V}$  to  $-1 \text{ V}$ ) where the plating and stripping processes occur. This strongly suggests an (electro)chemically induced phase transition taking place in the electrolyte during the plating/stripping process resulting in increased viscosity. This type of

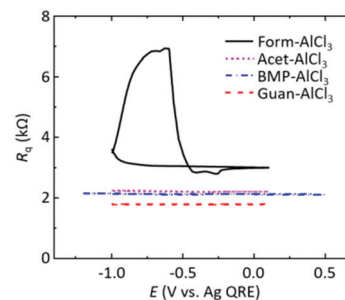


Fig. 2 Acoustic loss data (calculated from eqn (1)) as a function of potential for the different electrolytes.

behaviour has been reported for the electrodeposition of  $\text{Ti}$ ,<sup>26</sup>  $\text{Si}$ ,<sup>27</sup> and  $\text{Pb}$ <sup>28</sup> in IL-based systems.

The ionic conductivities ( $\sigma$ ) of the electrolytes were also determined *via* mathematical fitting (see ESI† 5) of the observed currents to eqn (2), as shown previously<sup>29</sup> from the stripping (*i.e.* anodic scan) portion of the  $i$ - $E$  curves.

$$i = \frac{\sigma \phi i_0 \left( \exp\left(\frac{nF(1-\alpha)\phi}{RT}\right) - \exp\left(\frac{-nF\alpha\phi}{RT}\right) \right)}{\sigma \phi + i_0 \left( \exp\left(\frac{nF(1-\alpha)\phi}{RT}\right) - \exp\left(\frac{-nF\alpha\phi}{RT}\right) \right)} \quad (2)$$

For comparative purposes, the fitting potential range is truncated to fit data between  $-1.0 \text{ V}$  and  $-0.53 \text{ V}$ , which is characteristic for all four electrolytes. This fitting is operable for a two-component system. Fig. 3 shows the anodic stripping curve for Guan- $\text{AlCl}_3$  (black dashed trace) and the corresponding fit (red solid trace) to eqn (2). It can be seen that the mathematical fit matches well to the experimental curve over the selected potential range, and this method allows estimation of the electrolyte conductivity. Using this approach we find conductivities on the order of  $10$ – $14 \text{ mS cm}^{-1}$  for the amidine electrolytes and  $6.5 \text{ mS cm}^{-1}$  for BMP- $\text{AlCl}_3$  (refer to Table 2). Other aluminium-based ILA electrolytes have shown room temperature conductivities of  $1$ – $1.5 \text{ mS cm}^{-1}$  (urea),<sup>13</sup>  $0.8 \text{ mS cm}^{-1}$  (acetamide),<sup>22</sup>  $5 \text{ mS cm}^{-1}$  (pyrrolidinium),<sup>10</sup> and  $10$ – $20 \text{ mS cm}^{-1}$  (imidazolium).<sup>7,8,10</sup> The conductivities of the amidine electrolytes are performing as good as state-of-the-art imidazolium-based ILAs and at a fraction of the economic cost.

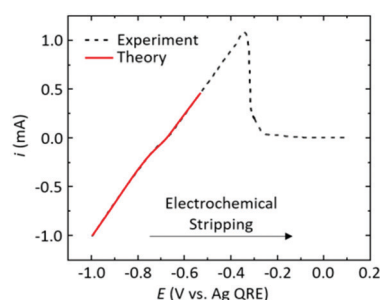


Fig. 3 Experimental voltammetric (anodic) stripping curve (black dashed trace) for Guan- $\text{AlCl}_3$  and the corresponding fit (red solid trace) to eqn (2). Refer to ESI† 5 for further details.



**Table 2** Room temperature conductivity, viscosity, and temperature-dependent (301–367 K) activation energies for viscous flow

Electrolyte	$\sigma/\text{ms cm}^{-1}$	$\eta/\text{cP}$	$E_a(\eta)/\text{kJ mol}^{-1}$
Guan- $\text{AlCl}_3$	14.2	51	8.9
Acet- $\text{AlCl}_3$	9.7	77	4.8
Form- $\text{AlCl}_3$	11.2	80	—
BMP- $\text{AlCl}_3$	6.5	60	9.7

For reference, the current prices of the different Lewis basic salts are provided in ESI† 1, and highlight that the Guan-Cl salt is highly cost-effective which is advantageous for scale-up.

The QCM set-up also allows the simultaneous estimation the electrolyte viscosity. Using the relationship in eqn (3):

$$R_q = [(\omega\eta\rho)/2]^{1/2} \quad (3)$$

where  $\omega (= 2\pi f)$  is the QCM frequency,  $\eta$  is the dynamic viscosity ( $\text{g cm}^{-1} \text{s}^{-1}$ ) and  $\rho$  is the density ( $\text{g cm}^{-3}$ ).<sup>24</sup> Again, water can be used as a calibration reference to estimate the viscosity of the ILA electrolytes. Specifically, this is accomplished by setting eqn (3), written for the ILA divided by eqn (3) again but written for water and solving for  $\eta_{\text{ILA}}$ . This method uses  $\rho_{\text{ILA}} = 1.3 \text{ g cm}^{-3}$ ,  $\eta_{\text{water}} = 0.01 \text{ g cm}^{-1} \text{s}^{-1}$  and  $\rho_{\text{water}} = 1 \text{ g cm}^{-3}$ . Accordingly, we find viscosities of  $0.51 \text{ g cm}^{-1} \text{s}^{-1}$  (Guan- $\text{AlCl}_3$ ),  $0.77 \text{ g cm}^{-1} \text{s}^{-1}$  (Acet- $\text{AlCl}_3$ ),  $0.80 \text{ g cm}^{-1} \text{s}^{-1}$  (Form- $\text{AlCl}_3$ ) and  $0.60 \text{ g cm}^{-1} \text{s}^{-1}$  (BMP- $\text{AlCl}_3$ ). Viscosity values are converted to centipoise (cP) in Table 2. This methodology was further used to determine viscosities over a range of temperatures (301–367 K) and the resultant Arrhenius plots (see ESI† 6, Fig. S5) yielded the activation energies for viscous flow, Table 2. These values are consistent with bulk measurements, but importantly, the Guan- $\text{AlCl}_3$  has the lowest viscosity of this series. For reference, other aluminium-based ILA electrolytes have 133 cP (urea),<sup>13</sup> 60 cP (acetamide),<sup>22</sup> 15 cP (imidazolium),<sup>10</sup> and 40–60 cP (pyrrolidinium).<sup>10</sup> Thus, the viscosity values of the amidine electrolytes are comparable to BMP- $\text{AlCl}_3$  and are significantly lower than values reported for amide-based systems.

In conclusion, the best performance was achieved with Guan- $\text{AlCl}_3$ , which has the highest concentration of  $\text{Al}^{3+}$  species, the highest ionic conductivity, and the lowest viscosity of the electrolytes explored here. In addition, the high Al concentration and low viscosity with Guan- $\text{AlCl}_3$  accounts for the facile electrochemical response and may contribute to the early onset reduction potential. Importantly, the Guan- $\text{AlCl}_3$  liquid is not only the best performing electrolyte of this series but it can also compete with current state-of-the-art imidazolium- and pyrrolidinium-based electrolytes at a significantly lower economic cost of the starting materials. Overall, this work represents a marked improvement on electrolyte development for Al battery chemistries. Future work will examine the compositional make-up of the amidine electrolytes, in addition to studying their plating characteristics.

This work was funded by the EU H2020-FETOPEN-1-2016-2017 G.A. 766581 SALBAGE and FETPROACT-EIC-06-2019 G.A. 951902 AMAPOLA projects.

## Conflicts of interest

There are no conflicts to declare.

## References

- D. Carrasco-Busturia, S. Lysgaard, P. Jankowski, T. Vegge, A. Bhowmik and J. M. Garcia-Lastra, *ChemSusChem*, 2021, **14**, 2034–2041.
- Á. Miguel, R. P. Fornari, N. García, A. Bhowmik, D. Carrasco-Busturia, J. M. Garcia-Lastra and P. Tiemblo, *ChemSusChem*, 2020, **13**, 5523–5530.
- G. Harper, R. Sommerville, E. Kendrick, L. Driscoll, P. Slater, R. Stolkin, A. Walton, P. Christensen, O. Heidrich, S. Lambert, A. Abbott, K. Ryder, L. Gaines and P. Anderson, *Nature*, 2019, **575**, 75–86.
- G. A. Elia, K. V. Kravchyk, M. V. Kovalenko, J. Chacón, A. Holland and R. G. A. Wills, *J. Power Sources*, 2021, **481**, 228870.
- K. V. Kravchyk and M. V. Kovalenko, *Commun. Chem.*, 2020, **3**, 120.
- B. Craig, T. Schoetz, A. Cruden and C. Ponce de Leon, *Renewable Sustainable Energy Rev.*, 2020, **133**, 110100.
- C. Ferrara, V. Dall'Asta, V. Berbenni, E. Quartarone and P. Mustarelli, *J. Phys. Chem. C*, 2017, **121**, 26607–26614.
- H. Wang, S. Gu, Y. Bai, S. Chen, N. Zhu, C. Wu and F. Wu, *J. Mater. Chem. A*, 2015, **3**, 22677–22686.
- M.-C. Lin, M. Gong, B. Lu, Y. Wu, D.-Y. Wang, M. Guan, M. Angell, C. Chen, J. Yang, B.-J. Hwang and H. Dai, *Nature*, 2015, **520**, 324–328.
- G. Zhu, M. Angell, C.-J. Pan, M.-C. Lin, H. Chen, C.-J. Huang, J. Lin, A. J. Achazi, P. Kaghazchi, B.-J. Hwang and H. Dai, *RSC Adv.*, 2019, **9**, 11322–11330.
- G. Pulletikurthi, B. Bödecker, A. Borodin, B. Weidenfeller and F. Endres, *Prog. Nat. Sci.: Mater. Int.*, 2015, **25**, 603–611.
- J.-P. M. Veder, M. D. Horne, T. Rütger, A. M. Bond and T. Rodopoulos, *Electrochim. Commun.*, 2013, **37**, 68–70.
- M. Angell, G. Zhu, M.-C. Lin, Y. Rong and H. Dai, *Adv. Funct. Mater.*, 2020, **30**, 1901928.
- K. L. Ng, M. Malik, E. Buch, T. Glossmann, A. Hintennach and G. Azimi, *Electrochim. Acta*, 2019, **327**, 135031.
- H. Jiao, C. Wang, J. Tu, D. Tian and S. Jiao, *Chem. Commun.*, 2017, **53**, 2331–2334.
- A. P. Abbott, R. C. Harris, Y.-T. Hsieh, K. S. Ryder and I. W. Sun, *Phys. Chem. Chem. Phys.*, 2014, **16**, 14675–14681.
- D. Paterno, E. Rock, A. Forbes, R. Iqbal, N. Mohammad and S. Suarez, *J. Mol. Liq.*, 2020, **319**, 114118.
- W. Chu, X. Zhang, J. Wang, S. Zhao, S. Liu and H. Yu, *Energy Storage Mater.*, 2019, **22**, 418–423.
- N. Canever, N. Bertrand and T. Nann, *Chem. Commun.*, 2018, **54**, 11725–11728.
- P. Hu, R. Zhang, X. Meng, H. Liu, C. Xu and Z. Liu, *Inorg. Chem.*, 2016, **55**, 2374–2380.
- M. Li, B. Gao, C. Liu, W. Chen, Z. Shi, X. Hu and Z. Wang, *Electrochim. Acta*, 2015, **180**, 811–814.
- H. M. A. Abood, A. P. Abbott, A. D. Ballantyne and K. S. Ryder, *Chem. Commun.*, 2011, **47**, 3523–3525.
- P. Giridhar, S. Zein El Abedin and F. Endres, *Electrochim. Acta*, 2012, **70**, 210–214.
- D. Johannsmann, *The Quartz Crystal Microbalance in Soft Matter Research: Fundamentals and Modeling*, Springer, Switzerland, 2015.
- A. R. Hillman, *J. Solid State Electrochem.*, 2011, **15**, 1647–1660.
- F. Endres, S. Zein El Abedin, A. Y. Saad, E. M. Moustafa, N. Borissenko, W. E. Price, G. G. Wallace, D. R. MacFarlane, P. J. Newman and A. Bund, *Phys. Chem. Chem. Phys.*, 2008, **10**, 2189–2199.
- J. Komadina, T. Akiyoshi, Y. Ishibashi, Y. Fukunaka and T. Homma, *Electrochim. Acta*, 2013, **100**, 236–241.
- Y. Katayama, R. Fukui and T. Miura, *J. Electrochem. Soc.*, 2013, **160**, D251–D255.
- T. Schoetz, O. M. Leung, I. Efimov, C. Zaleski, Á. M. Ortega, N. G. García, P. Tiemblo Magro and C. Ponce de Leon, *J. Electrochem. Soc.*, 2020, **167**, 089006.

